Published in final edited form as:
Mol Immunol. 2014 February ; 57(2): . doi:10.1016/j.molimm.2013.10.007.

Membrane Pore Formation by Human Complement: Functional Importance of the Transmembrane β-Hairpin (TMH) Segments of C8α and C9

Mitch H. Weiland[a,b], **Yu Qian**[a,c], and **James M. Sodetz**[a,d]

[a]Department of Chemistry and Biochemistry, University of South Carolina, Columbia, SC 29208 USA

Abstract

Human C8 and C9 have a key role in forming the pore-like "membrane attack complex" (MAC) of complement on bacterial cells. A possible mechanism for membrane insertion of these proteins was suggested when studies revealed a structural similarity between the MACPF domains of the C8α and C8β subunits and the pore-forming bacterial cholesterol-dependent cytolysins (CDCs). This similarity includes a pair of α-helical bundles that in the CDCs refold during pore formation to produce two transmembrane β-hairpins (TMH1 and TMH2). C9 is the major pore-forming component of the MAC and is also likely to contain two TMH segments because of its homology to C8α and C8β. To determine their potential for membrane insertion, the TMH sequences in C8α and those predicted to be in C9 were substituted for the TMH sequences in perfringolysin O (PFO), a well-characterized CDC. Only chimeric proteins containing TMH2 from C8α (PFO/αT2) or C9 (PFO/C9T2) could be expressed in soluble, active form. The PFO/αT2 and PFO/C9T2 chimeras retained significant hemolytic activity, formed pore-like structures on membranes, and could combine with PFO to form hemolytically active mixed complexes that were functionally similar to PFO alone. These results provide experimental evidence in support of the hypothesis that TMH segments in C8α and those predicted to be in C9 have a direct role in MAC membrane penetration and pore formation.

Keywords

complement; C8; C9; perfringolysin O; MACPF; membrane attack complex

1. INTRODUCTION

The human complement system functions to eliminate gram-negative bacteria and other foreign pathogens by forming a pore-like "membrane attack complex" (MAC) on target cell membranes. This complex is composed of complement proteins C5b, C6, C7, C8, and C9 [1–3]. Assembly of the first four components leads to formation of C5b-8, which acts as a receptor for C9. Subsequent binding of multiple C9 molecules produces a cylindrical

[d]To whom correspondence should be addressed: jsodetz@mailbox.sc.edu, Tel: 803-777-6625, Fax: 803-777-9521.
[b]Present address: Department of Chemistry and Physics, Armstrong Atlantic State University, Savannah, GA 31419 USA
[c]Present address: Department of Chemistry, Boston College, Chestnut Hill, MA 02467 USA

transmembrane pore composed of 12–18 C9s. C8 is a trimeric protein composed of a C8α, C8β, and C8γ subunit, each produced from a separate gene [4,5]. The C8α and C8β subunits along with C6, C7, and C9 are homologous and constitute the "MAC family" of proteins [6,7]. MAC family members contain disulfide rich modules at the N- and C-termini and a central ~40 kDa membrane attack complex/perforin (MACPF) domain.

Several hundred MACPF-containing proteins have been identified based on their signature MACPF motif (Y/W-G-T/S-H-F/Y-X_6-G-G) [8]. They exhibit limited sequence similarity and with a few exceptions, such as the MAC proteins and perforin [9], their function is unknown. Crystal structures of several MACPF-containing proteins including perforin, C6, and C8 revealed a fold similar to the cholesterol-dependent cytolysins (CDCs), a family of pore-forming bacterial toxins [10–16]. The core structure of the MACPF/CDC domain consists of a distinctive L-shaped four-stranded antiparallel β-sheet flanked by two α-helical bundles. During CDC pore formation, ~30–50 CDC monomers assemble on cholesterol-rich regions of the cell surface to form an oligomeric prepore [17,18]. Adjacent monomers align through stacking of aromatic residues in β-strand 4 of one CDC molecule with β-strand 1 of another [19]. β-strand alignment directs refolding of the two α-helical bundles in each monomer to form two amphipathic transmembrane β-hairpins (TMH), hence the two α-helical bundles are referred to as TMH1 and TMH2 [20,21]. In a concerted manner, aligned TMHs from each monomer are inserted into the membrane to form a transmembrane β-barrel pore [22]. Conservation of core structural features suggests the two α-helical bundles in the MAC proteins function like TMHs in the CDCs and facilitate anchoring of the MAC to the membrane and formation of the MAC pore [23].

The mechanism of pore formation by CDCs has been extensively studied using the toxin perfringolysin O (PFO) from *Clostridium perfringens* (18). Models of pre-pore and pore formation have been developed and the PFO segments that insert into membranes identified [19–21]. By contrast, those segments of the MAC proteins that penetrate or traverse the membrane bilayer are unknown. In the present study, we examined whether the putative TMH segments of C8α and C9 have the potential to function like TMHs in the CDCs. C8α and C9 were chosen for study because photolabeling studies found that these two MAC proteins are the predominant ones inserted into the membrane [24]. Also, C9 is known to be the major pore-forming component of the MAC [25]. We used PFO as a platform to produce chimeric proteins in which TMH segments of PFO were replaced with the TMH segments of C8α or with those predicted to be in C9 based on sequence homology. Only chimeras containing TMH2 from C8α (PFO/αT2) or C9 (PFO/C9T2) could be expressed in soluble, active form. Both chimeras had significant hemolytic activity, formed pore-like structures on membranes, and could combine with PFO to form hemolytically active mixed complexes that were functionally similar to PFO alone. Together, these results support the hypothesis that TMHs in C8α and those predicted to be in C9 have a direct role in MAC membrane penetration and pore formation.

2. MATERIALS AND METHODS

2.1 Expression and Purification of PFO

The pRT20 plasmid encoding perfringolysin O (PFO^{C459A}) was a generous gift from Dr. Rodney K. Tweten, University of Oklahoma [19]. PFO^{C459A} contains an N-terminal 6xHis tag, retains the same activity and characteristics of native PFO, and will be referred to as PFO. Expression and purification followed the procedure by Shepard et. al. [19], with the following modifications. The pRT20 plasmid was transformed into Origami B(DE3) (Novagen) expression cells. Bacteria were grown in LB-carbenicillin Media (1% Bacto tryptone (w/v), 0.5% Bacto yeast extract (w/v), 171 mM NaCl, 50 μg/mL carbenicillin) to an $O.D._{600}$ = 0.5, induced with 1 mM IPTG, and proteins were expressed at 37°C for 3hr. Cells

were harvested by centrifugation and lysed using BugBuster HT protein extraction reagent (Novagen) containing 5% (v/v) Triton X-100, 0.1 mg/mL lysozyme, and the protease inhibitors AEBSF (1 mM) and E-64 (10 μM) (Calbiochem). The supernatant was then applied to a Ni-NTA Superflow column (Qiagen) and the column washed with 50 mM Tris-HCl, 300 mM NaCl, and 20 mM imidazole, pH 8.0. Bound PFO was eluted in a 20–500 mM imidazole gradient in the same buffer. Fractions containing pure PFO were dialyzed against 50 mM sodium phosphate and 150 mM NaCl, pH 7.4 and stored in 10% (v/v) glycerol at −70 °C.

2.2 Cloning of PFO Chimeras

Expression plasmids were created using the pRT20 backbone, which had a silent mutation introduced to remove an internal NdeI site. C8αMACPF/pMCSG7 [26] and human C9/pET12b (a generous gift from Alfred Esser, University of Missouri, Kansas City) were used as templates to create the C8αTMH and C9TMH PCR products. Substitution of the TMH segments was accomplished using overlap extension (OLE) PCR. The 5′ and 3′ primers were designed to incorporate NdeI and XhoI sites, respectively. OLE-PCR products were digested and ligated into pET17b. To eliminate intermolecular crosslinking and increase protein yields, the Quik Change protocol (Stratagene) was used to introduce two Cys to Ala mutations in the chimeric constructs. These residues correspond to Cys 346/370 in C8α and Cys 350/385 in C9. Experiments performed with the Cys intact showed no difference in activity (data not shown); therefore, all experiments were performed using the cysteine-less constructs. Plasmids were transformed into Origami B (DE3) cells (Novagen) for expression.

2.3 Expression and Purification of PFO Chimeras

Expression conditions and purification methods were the same for all chimeric proteins. Bacteria were grown in LB-carbenicillin media to an $O.D._{600}$ = 1.0, induced with 1 mM final IPTG, and expressed at 30°C for 4 hrs. Cells were harvested, lysed and applied to a Ni-NTA column using the procedure for PFO. Fractions eluted from the Ni-NTA column were concentrated and the NaCl diluted to 50 mM using 50 mM Tris-HCl, pH 8.0. Samples were then applied to a 1mL HiTrap Q XL anion exchange column. The column was washed with 50 mM Tris-HCl, 50 mM NaCl, pH 8.0 and eluted with a 0.05–1.0 M NaCl gradient in the same buffer. Concentrations of final products were determined using theoretical extinction coefficients.

2.4 Hemolytic Activity of Chimeras

Hemolytic activity was determined by the amount of protein necessary for 50% hemolysis using a modified published procedure [27]. Rabbit erythrocytes (Lampire Biological Laboratories, USA) were washed and resuspended to 1×10^8 cells/mL with hemolytic assay buffer (50 mM sodium phosphate, 150 mM NaCl, 0.1 mg/ml BSA, pH 7.5). Assays contained 140 μL hemolytic assay buffer, 35 μL of erythrocytes suspension and 50 μl of protein dilution. Following incubation at 37 °C for 35 minutes, samples were centrifuged and hemolysis was determined by measuring the released hemoglobin at 405 nm. Hemolysis control values were obtained by adding 35 μl erythrocytes suspension into 190 μl water or assay buffer.

2.5 Rabbit Ghost Membrane Preparation

Packed rabbit erythrocytes were lysed by the addition of 50x (v/v) cold 5 mM sodium phosphate buffer, pH 7.5 to yield membrane ghosts. Following lysis, hemoglobin was separated from the membranes using the Vivaflow 200 system (Sartorius Stedim Biotech GmbH, Germany) according to manufacturer's instructions. Ghosts were pelleted at 30,000

x g, resuspended in 50 mM Tris-HCl, 150 mM NaCl, pH 8.0, and the concentration determined by Bradford assay.

2.6 Transmission Electron Microscopy

Protein solutions (~600 nM) in buffer (50 mM Tris-HCl, 150 mM NaCl, pH 8.0) were incubated with 10 μg ghost membranes in 100 μl buffer at 37 °C for 40 minutes. Following incubation, samples were pipetted on parafilm as 30 μl droplets. Formvar-carbon grids were floated on the sample for 3 minutes and negatively stained with 5% (w/v) uranyl acetate for 5 minutes. Samples were then examined and photographed on a Hitachi H8000 transmission electron microscope operated at 200 kV.

2.7 Enterokinase cleavage of PFO

PFO expressed from the pRT20 vector contains an additional 36 N-terminal residues (MGGSHHHHHHGMASMTGGQQMGRDLYDDDDKDRWGS) which codes for a 6x His tag and an enterokinase cleavage site (underlined). To discriminate between PFO and His-tagged chimeras in immunoblots the N-terminal PFO tag containing the enterokinase site was removed using a recombinant enterokinase kit (Novagen). Cleaved PFO was applied to a Ni-NTA column in 50 mM Tris-HCl, 150 mM NaCl, pH 8.0 and the flow through was collected. SDS-PAGE analysis showed a homogeneous cleaved PFO product (data not shown).

2.8 Agarose Gel Electrophoresis and Immunoblot Analysis

Denaturing agarose gel electrophoresis (SDS-AGE) was carried out using published procedures [28]. PFO/αT2 or PFO/C9T2 was pre-mixed with reaction buffer (50 mM sodium phosphate, 150 mM NaCl, pH 7.4) or with excesses of enterokinase cleaved PFO. Rabbit ghost membranes (0.3 μg/μL) were added to chimeric protein samples and incubated at 37°C for 30 minutes. Reactions were stopped by the addition of 5% (w/v) SDS, 10% (v/v) glycerol, 0.01% (w/v) bromophenol blue in chamber buffer (25 mM Tris-HCl, 192 mM glycine, 0.1% SDS (w/v). Samples were loaded onto a 1.0% SeaPlaque GTG Agarose (Lonza) gel (prepared by melting the agarose at 100 °C in chamber buffer and pouring into a horizontal gel casting tray) and separated for 45–50 minutes at 100 V. Proteins were transferred to nitrocellulose using a Bio-Rad Trans-Blot Cell. Chimeras were detected using a 1° Monoclonal Anti-His Antibody (Genescript) and 2° IRDye 800CW (Licor). Blots were imaged using an Odyssey Infrared Imaging System (Licor).

2.9 Activity of Mixed Complexes of Chimeras and PFO

To determine if complexes of chimera and PFO were active, hemolytic assays were performed in which PFO was held at a fixed, sublytic level that showed no detectable activity (PFO_0). Increasing amounts of either chimera or PFO control, which were also at sublytic levels, were then added to PFO_0. Pre-incubations consisted of 30 μL of PFO_0(0.12 pg/μL) with 30 μL of chimera or PFO at 25 °C for 15 min. The mixture was then added to 175 μL of rabbit erythrocytes (2.0×10^7 cells/mL) and incubated at 37 °C for 35 min before measuring hemolysis.

3. RESULTS

3.1 Production and Hemolytic Activity of PFO Chimeras

Comparison of the PFO and MACPF domains of C8α and C8β shows a conserved antiparallel β-sheet structure flanked by two α-helical bundles (Fig. 1). In PFO, the α-helical bundles refold to form transmembrane β-hairpins. To determine if the putative TMH regions within the complement proteins are capable of functioning as replacements for the PFO

TMHs, a series of chimeras were created by substituting one or both PFO TMH segments with corresponding ones from C8α or C9. Of the chimeras created, only PFO/αT2 and PFO/C9T2 could be expressed in a soluble, active form (Table 1). These two chimeras exhibited 10–15% of the hemolytic activity of PFO (Fig. 2). The TMH2 segments of C8α and C9 are significantly larger than PFO TMH2 (57 and 58 residues for C8α and C9, respectively; 32 residues for PFO) and this may contribute to the lower activity. Based on the model for CDC pore formation [18,23], these results suggest the C8α and C9 TMH2s can substitute for PFO TMH2 and hydrogen bond with PFO TMH1 to form a functional pore.

3.2 PFO/αT2 and PFO/C9T2 Form Pore-like Structures on Membranes

To determine if the hemolytic activity of PFO/αT2 and PFO/C9T2 correlates with formation of pore-like structures on membranes, EM images were obtained of rabbit ghost membranes that were incubated with PFO or the chimeras (Fig. 3). PFO forms well-defined concentric pores with an average outside diameter of ~30–40nm, in good agreement with previous reports [22,29,30]. Corresponding images of PFO/αT2 and PFO/C9T2 also show pore-like structures but of a larger diameter (~50–60nm). For both chimeras, the near doubling in size of their pore-like structures relative to PFO is likely due to the longer C8α and C9 TMH2 segments distorting oligomer packing.

3.3 PFO/αT2 and PFO/C9T2 form SDS-Resistant Oligomers with PFO

Oligomers of PFO formed on cholesterol rich membranes have been shown to resist dissociation in the presence of SDS. Such resistant oligomers can be examined using SDS-AGE and immunoblotting [28]. To determine if the chimeras form SDS-resistant oligomers on membranes, oligomer formation was examined by SDS-AGE in the absence and presence of enterokinase-cleaved PFO (Fig. 4). Results show PFO/αT2 alone does not form SDS-resistant oligomers in the absence or presence of ghost membranes. However, addition of PFO enables PFO/αT2 to co-incorporate into mixed oligomers that are SDS-resistant. Co-incorporation can be detected at a 1:1 ratio of PFO:PFO/αT2 and is nearly complete with a 20-fold excess of PFO. Similar experiments with PFO/C9T2 show that PFO/C9T2 forms a significant amount of SDS-resistant oligomers in the absence of PFO. A large portion of PFO/C9T2 becomes incorporated when mixed with a 1:1 ratio of PFO, and incorporation is nearly complete with only a 5-fold excess of PFO.

3.4 PFO/αT2 or PFO/C9T2 Incorporates with PFO to Form Hemolytically Active Complexes

Hemolytic assays were performed to determine if the mixed oligomers formed with the chimeras and PFO are active. In these experiments (Fig. 5), a fixed amount of PFO was used at a sublytic level (PFO_0) that produced no detectable hemolysis. Increasing amounts of PFO/αT2 or PFO/C9T2 were then added at levels which were also sublytic when assayed alone. When sublytic amounts of chimera were mixed with sublytic PFO_0, hemolytic activity could be detected. Importantly, for both chimeras the activity of the mixed complexes was similar to that of a PFO control up to ~20% lysis. As expected, the activity of the PFO control continues to increase as more is added whereas with the chimeras the activity levels off at ~15–20%. This is expected because the chimeras are not as active as PFO and at higher levels they become the major component in the mixed complexes. These results show that both chimeras can co-incorporate with PFO to form active, mixed complexes and when incorporated at lower molar ratios these complexes are functionally similar to those formed solely with PFO.

4. DISCUSSION

The close similarity between core structural features of the CDCs and C8α and C8β renders it likely that membrane anchoring and insertion of the MAC is mediated by refolding of the

α-helical bundles TMH1 and TMH2 into β-hairpins that either partially penetrate or fully traverse the membrane. The homology to C8α and C8β suggests that C9 also contains a pair of α-helical bundles that refold and facilitate pore formation by poly C9 in the fully assembled MAC. From the structure of C8 and the unusual geometrical relationship between C8α and C8β, a model was proposed that describes how the MAC might assemble to form a circular pore [15]. A more recent and detailed model of how C5b, C6, C7 and C8 interact to form C5b-8 and conformational changes that would allow refolding of the α-helical bundles was described based on structures of C6 and C8 [16]. Although the role of the TMHs in CDC pore formation is clearly established, there currently is no experimental evidence that a similar refolding occurs for the MAC proteins nor that their putative TMHs are capable of membrane insertion.

Photolabeling studies directed towards identifying MAC proteins that insert into the membrane bilayer determined that C8α and C9 are the major membrane-inserting components [24]. For C9, efforts to identify the portion(s) inserted have yielded conflicting results. Photolabeling studies of the MAC using membrane-restricted probes found that only the hydrophobic C9b fragment (residues 245–538) of C9 was labeled [31]. Subsequent photolabeling and proteolytic digestion experiments reported the membrane interacting region to be within C9 residues 176–345 [32]. Using secondary structure predictions, it was proposed that this region was a helix-turn-helix comprised of C9 residues 292–334 with 309–313 being the turn. Rossi et al [33] subsequently refuted this prediction by introducing a N-linked glycosylation site, K311N, in the middle of the predicted turn region. This mutant was shown to be glycosylated and retain hemolytic activity. Movement of an N-linked carbohydrate across a lipid bilayer is energetically unfavorable and unlikely to occur. Additionally, if the predicted C9 core structure is similar to C8α, then the region suggested by Pietsch et al.[32] would indeed be a helix-turn-helix, but it would correspond to the D and E helices located near the top of the C8α MACPF domain and away from the TMHs.

Our results provide experimental support for TMH involvement in MAC pore formation. Although chimeric PFO constructs containing TMH1 or TMH1 + TMH2 from C8α or C9 could not be produced in active form, the respective TMH2s were shown to be effective substitutes for PFO TMH2. Chimeras containing C8α or C9 TMH2s form circular pore-like structures on membranes and retain ~10–15% of the hemolytic activity of PFO. The observed pore-like structures have nearly twice the diameter of PFO pores, most likely because the longer C8α and C9 TMH2s cannot optimally align with PFO TMH1 in the oligomer. The disrupted packing also alters the SDS resistance normally observed with PFO, as oligomers formed with the C8α chimera showed no SDS-resistance and only slight resistance was seen for the C9 chimera. Interestingly, the absence of SDS-resistance was also seen with a PFO^{Y181A} mutant [22]. This construct was shown to oligomerize but then is trapped in the pre-pore conformation. Adding wild-type PFO to PFO^{Y181A} induces a conformational change sufficient to overcome the raised energy barrier imparted by the mutation, thereby allowing PFO^{Y181A} to form SDS-resistant complexes and insert its β-hairpins into a membrane. Similarly, addition of PFO to the C8α and C9 TMH2 chimeras resulted in formation of SDS-resistant oligomers. Complete SDS-resistance of the C8α chimera was observed with a 20-fold excess of PFO whereas only a 5-fold excess of PFO was needed for the C9 TMH2 chimera. This difference suggests that compared to C8α the TMH2 of C9 can refold and align better with PFO TMH1. Such a result would be consistent with the role of C9 as the major pore-forming component of the MAC.

Further support for the C8α and C9 TMH2s as effective replacements for PFO TMH2 is seen with activity assays performed by mixing PFO with the C8α and C9 chimeras. At low molar excesses, PFO/αT2 or PFO/C9T2 can combine with PFO to form functional complexes with activities similar to PFO alone. As expected, when the proportion of

chimera in the complexes increases, the activity levels off because the chimeras alone are less active than PFO. Results obtained at the lower molar ratios are significant because they indicate the C8α and C9 TMH2s are capable of interacting with the TMH1 of PFO to form a functional pore. This supports the likelihood that similar interactions between the TMH1s and TMH2s of C8α and/or C9 have a role in anchoring the MAC to the membrane and in pore formation.

In conclusion, we have shown that TMHs in the complement pore-forming proteins have the potential to function like the TMHs in the CDCs. The chimeras PFO/αT2 and PFO/C9T2 alone formed pore-like structures capable of lysing cell membranes and both could associate with PFO to form functional, mixed complexes. While our results do not allow a detailed comparison between the mechanisms used by the MAC and CDCs to form pores, they do provide the first experimental evidence that TMHs in C8α and C9 have a direct role.

Acknowledgments

We thank Dr. Rodney Tweten for providing the pRT20 plasmid and Dr. Alfred Esser for the human C9/pET12b plasmid. We also thank the University of South Carolina Electron Microscopy Center for use of the EM instrument and Dr. Soumitra Ghoshroy for scientific and technical assistance with the EM experiments. This work was supported by NIH Grant GM042898.

References

1. Müller-Eberhard HJ. Molecular organization and function of the complement system. Annu Rev Biochem. 1988; 57:321–347. [PubMed: 3052276]
2. DiScipio RG. The relationship between polymerization of complement component C9 and membrane channel formation. J Immunol. 1991; 147:4239–4247. [PubMed: 1721643]
3. Esser AF. The membrane attack complex of complement. Assembly, structure and cytotoxic activity Toxicology. 1994; 87:229–247.
4. Steckel EW, York RG, Monahan JB, Sodetz JM. The eighth component of human complement. Purification and physicochemical characterization of its unusual subunit structure. J Biol Chem. 1980; 255:11997–12005. [PubMed: 7440581]
5. Ng SC, Rao AG, Howard OM, Sodetz JM. The eighth component of human complement: evidence that it is an oligomeric serum protein assembled from products of three different genes. Biochemistry. 1987; 26:5229–5233. [PubMed: 3676249]
6. Hobart MJ, Fernie BA, DiScipio RG. Structure of the human C7 gene and comparison with the C6, C8A, C8B, and C9 genes. J Immunol. 1995; 154:5188–5194. [PubMed: 7730625]
7. Plumb, ME.; Sodetz, JM. Proteins of the membrane attack complex. In: Volanakis, JE.; Frank, MM., editors. The Human Complement System in Health and Disease. Marcel Dekker; New York: 1998. p. 119-148.
8. Ponting CP. Chlamydial homologues of the MACPF (MAC/perforin) domain. Curr Biol. 1999; 9:R911–R913. [PubMed: 10608922]
9. Pipkin ME, Lieberman J. Delivering the kiss of death: progress on understanding how perforin works. Curr Opin Immunol. 2007; 19:301–308. [PubMed: 17433871]
10. Hadders MA, Beringer DX, Gros P. Structure of C8αlpha-MACPF reveals mechanism of membrane attack in complement immune defense. Science. 2007; 317:1552–1554. [PubMed: 17872444]
11. Rosado CJ, Buckle AM, Law RH, Butcher RE, Kan WT, Bird CH, Ung K, Browne KA, Baran K, Bashtannyk-Puhalovich TA, Faux NG, Wong W, Porter CJ, Pike RN, Ellisdon AM, Pearce MC, Bottomley SP, Emsley J, Smith AI, Rossjohn J, Hartland EL, Voskoboinik I, Trapani JA, Bird PI, Dunstone MA, Whisstock JC. A common fold mediates vertebrate defense and bacterial attack. Science. 2007; 317:1548–1551. [PubMed: 17717151]
12. Slade DJ, Lovelace LL, Chruszcz M, Minor W, Lebioda L, Sodetz JM. Crystal structure of the MACPF domain of human complement protein C8 alpha in complex with the C8 gamma subunit. J Mol Biol. 2008; 379:331–342. [PubMed: 18440555]

13. Law RH, Lukoyanova N, Voskoboinik I, Caradoc-Davies TT, Baran K, Dunstone MA, D'Angelo ME, Orlova EV, Coulibaly F, Verschoor S, Browne KA, Ciccone A, Kuiper MJ, Bird PI, Trapani JA, Saibil HR, Whisstock JC. The structural basis for membrane binding and pore formation by lymphocyte perforin. Nature. 2010; 468:447–451. [PubMed: 21037563]

14. Xu Q, Abdubek P, Astakhova T, Axelrod HL, Bakolitsa C, Cai X, Carlton D, Chen C, Chiu HJ, Clayton T, Das D, Deller MC, Duan L, Ellrott K, Farr CL, Feuerhelm J, Grant JC, Grzechnik A, Han GW, Jaroszewski L, Jin KK, Klock HE, Knuth MW, Kozbial P, Krishna SS, Kumar A, Lam WW, Marciano D, Miller MD, Morse AT, Nigoghossian E, Nopakun A, Okach L, Puckett C, Reyes R, Tien HJ, Trame CB, van den BH, Weekes D, Wooten T, Yeh A, Zhou J, Hodgson KO, Wooley J, Elsliger MA, Deacon AM, Godzik A, Lesley SA, Wilson IA. Structure of a membrane-attack complex/perforin (MACPF) family protein from the human gut symbiont Bacteroides thetaiotaomicron. Acta Crystallogr Sect F Struct Biol Cryst Commun. 2010; 66:1297–1305.

15. Lovelace LL, Cooper CL, Sodetz JM, Lebioda L. Structure of human C8 protein provides mechanistic insight into membrane pore formation by complement. J Biol Chem. 2011; 286:17585–17592. [PubMed: 21454577]

16. Aleshin AE, Schraufstatter IU, Stec B, Bankston LA, Liddington RC, DiScipio RG. Structure of complement C6 suggests a mechanism for initiation and unidirectional, sequential assembly of membrane attack complex (MAC). J Biol Chem. 2012; 287:10210–10222. [PubMed: 22267737]

17. Tweten RK. Cholesterol-dependent cytolysins, a family of versatile pore-forming toxins. Infect Immun. 2005; 73:6199–6209. [PubMed: 16177291]

18. Hotze EM, Tweten RK. Membrane assembly of the cholesterol-dependent cytolysin pore complex. Biochim Biophys Acta. 2012; 1818:1028–38. [PubMed: 21835159]

19. Ramachandran R, Tweten RK, Johnson AE. Membrane-dependent conformational changes initiate cholesterol-dependent cytolysin oligomerization and intersubunit beta-strand alignment. Nat Struct Mol Biol. 2004; 11:697–705. [PubMed: 15235590]

20. Shepard LA, Heuck AP, Hamman BD, Rossjohn J, Parker MW, Ryan KR, Johnson AE, Tweten RK. Identification of a membrane-spanning domain of the thiol-activated pore-forming toxin Clostridium perfringens perfringolysin O: an alpha-helical to beta-sheet transition identified by fluorescence spectroscopy. Biochemistry. 1998; 37:14563–14574. [PubMed: 9772185]

21. Shatursky O, Heuck AP, Shepard LA, Rossjohn J, Parker MW, Johnson AE, Tweten RK. The mechanism of membrane insertion for a cholesterol-dependent cytolysin: a novel paradigm for pore-forming toxins. Cell. 1999; 99:293–299. [PubMed: 10555145]

22. Hotze EM, Heuck AP, Czajkowsky DM, Shao Z, Johnson AE, Tweten RK. Monomer-monomer interactions drive the prepore to pore conversion of a beta-barrel-forming cholesterol-dependent cytolysin. J Biol Chem. 2002; 277:11597–11605. [PubMed: 11799121]

23. Dunstone MA, Tweten RK. Packing a punch: the mechanism of pore formation by cholesterol dependent cytolysins and membrane attack complex/perforin-like proteins. Curr Opin Struct Biol. 2012; 22:342–349. [PubMed: 22658510]

24. Steckel EW, Welbaum BE, Sodetz JM. Evidence of direct insertion of terminal complement proteins into cell membrane bilayers during cytolysis. Labeling by a photosensitive membrane probe reveals a major role for the eighth and ninth components. J Biol Chem. 1983; 258:4318–4324. [PubMed: 6833260]

25. DiScipio RG, Berlin C. The architectural transition of human complement component C9 to poly(C9). Mol Immunol. 1999; 36:575–585. [PubMed: 10499811]

26. Slade DJ, Chiswell B, Sodetz JM. Functional studies of the MACPF domain of human complement protein C8alpha reveal sites for simultaneous binding of C8beta, C8gamma, and C9. Biochemistry. 2006; 45:5290–5296. [PubMed: 16618117]

27. Tweten RK. Cloning and expression in Escherichia coli of the perfringolysin O (theta-toxin) gene from Clostridium perfringens and characterization of the gene product. Infect Immun. 1988; 56:3228–3234. [PubMed: 2903127]

28. Shepard LA, Shatursky O, Johnson AE, Tweten RK. The mechanism of pore assembly for a cholesterol-dependent cytolysin: formation of a large prepore complex precedes the insertion of the transmembrane beta-hairpins. Biochemistry. 2000; 39:10284–10293. [PubMed: 10956018]

29. Hotze EM, Wilson-Kubalek EM, Rossjohn J, Parker MW, Johnson AE, Tweten RK. Arresting pore formation of a cholesterol-dependent cytolysin by disulfide trapping synchronizes the insertion of the transmembrane beta-sheet from a prepore intermediate. J Biol Chem. 2001; 276:8261–8268. [PubMed: 11102453]

30. Dang TX, Hotze EM, Rouiller I, Tweten RK, Wilson-Kubalek EM. Prepore to pore transition of a cholesterol-dependent cytolysin visualized by electron microscopy. J Struct Biol. 2005; 150:100–108. [PubMed: 15797734]

31. Ishida B, Wisnieski BJ, Lavine CH, Esser AF. Photolabeling of a hydrophobic domain of the ninth component of human complement. J Biol Chem. 1982; 257:10551–10553. [PubMed: 7107623]

32. Peitsch MC, Amiguet P, Guy R, Brunner J, Maizel JV Jr, Tschopp J. Localization and molecular modelling of the membrane-inserted domain of the ninth component of human complement and perforin. Mol Immunol. 1990; 27:589–602. [PubMed: 2395434]

33. Rossi V, Wang Y, Esser AF. Topology of the membrane-bound form of complement protein C9 probed by glycosylation mapping, anti-peptide antibody binding, and disulfide modification. Mol Immunol. 2010; 47:1553–1560. [PubMed: 20153530]

Highlights

- Function of the transmembrane β-hairpin (TMH) segments in C8α and C9 was examined.
- TMH segments from human C8α and C9 were inserted into perfringolysin O (PFO).
- Chimeras of PFO and C8α or C9 retained functional properties of wild-type PFO.
- C8α and C9 can form CDC-like transmembrane β-hairpins.

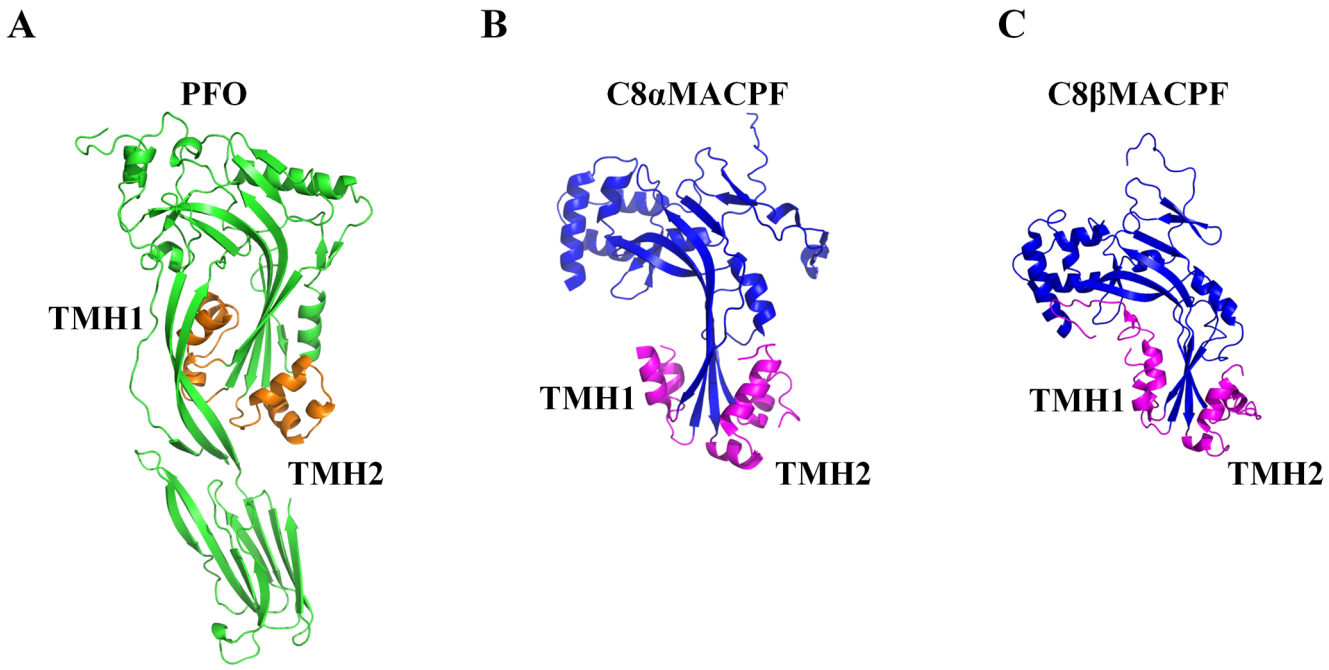


```
        PFO (158-191) VYSKSQISSALNVNAKVLENSLGVDFNAVANNEK
TMH1    C8α (201-256) DNANDLLSKVKKDKSDSFGVTIGIGPAGSPLL------------------VGVGVSHSQDTSFLNELNKYNEKK
        C8β (181-235) ESYSDFERNVTEKAMASKSGFSFGFKIPGI-FE-----------------LGISSQSDRGKHYIRRTKRFSHTK
        C9  (197-270) EEQIEAFKSIIQEKTSNFNAAISLKFTPTETNKAEQCCEETASSISLHGKGSFRFSYSKNETYQLFLSYSSKKE

        PFO (256-287) TSSSKDVQAAFKALIKNTDIKNSQQYKDIYEN
TMH2    C8α (329-385) KAKMESLGITSRDITTCFGGSLGIQYE-DKINVGGGLSGDHCKKFGGG-KT--ERARKAMA
        C8β (308-365) KEAMERGDYTLNNVHACAKNDFKIGGAIEEVYVSLGVSVGKCRGILNEIK---DRNKRDTM
        C9  (343-400) KASMKRKGVELKDIKRCLGYHLDVSLAFSEISVGAEFNKDDCVKRGEG-RA--VNITSENL
```

Fig. 1.

Structural comparison of PFO, C8αMACPF and C8βMACPF and sequence alignments of the TMHs. Residue numbers are for the full-length mature proteins. Shown are structures of PFO (PDB code: 1PFO) and the MACPF domains of C8α and C8β (PDB code: 3OJY). TMHs in PFO are colored in orange and TMHs in C8α and C8β are in magenta. Sequence alignments were used to predict the location of TMH segments in C9.

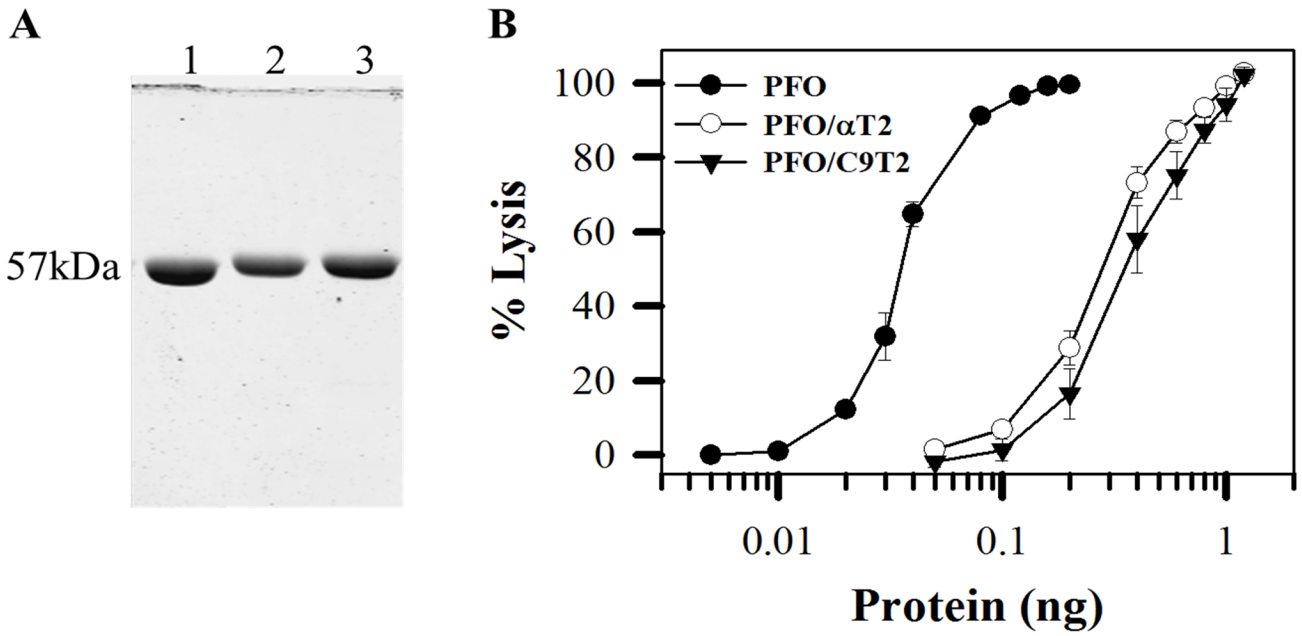

Fig. 2.

Purification and hemolytic activity of PFO, PFO/αT2 and PFO/C9T2.

(A) SDS-PAGE gel of non-reduced samples of PFO (Lane 1), PFO/αT2 (Lane 2) and PFO/C9T2 (Lane 3). The gel was stained with coomassie blue. The mobility difference between PFO and chimeras is due to the additional residues in the complement TMH2. (B) Hemolytic activity of PFO and the chimeras.

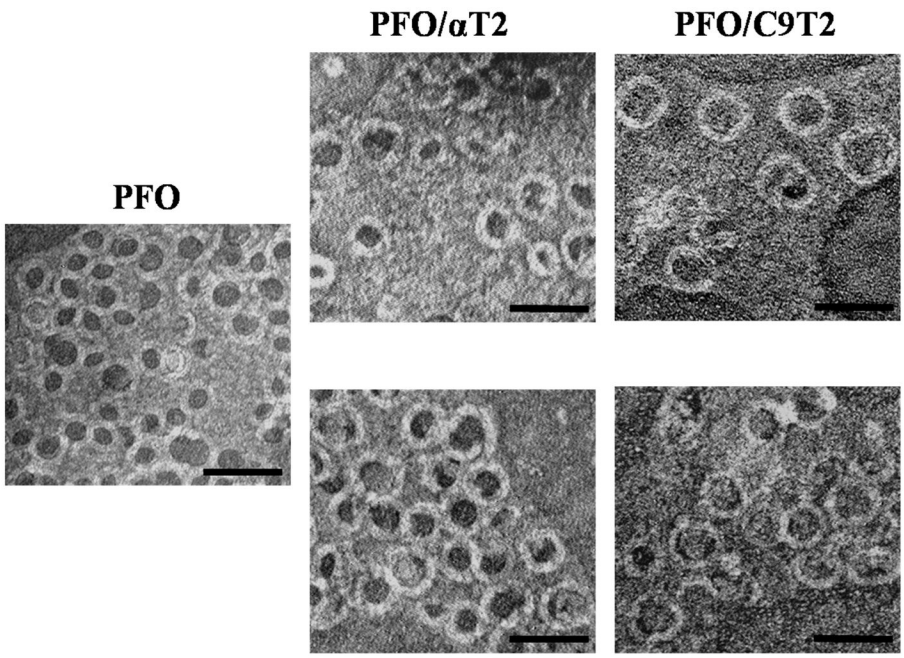

Figure 3.
EM images of rabbit erythrocyte ghost membranes incubated with PFO, PFO/αT2 or PFO/C9T2. Upper and lower panels are different images at the same magnification. Scale bar is 100 nm.

A

Lane	1	2	3	4	5
PFO(ng)	-	-	75	375	1500
PFO/αT2(ng)	75	75	75	75	75
Membrane	-	+	+	+	+

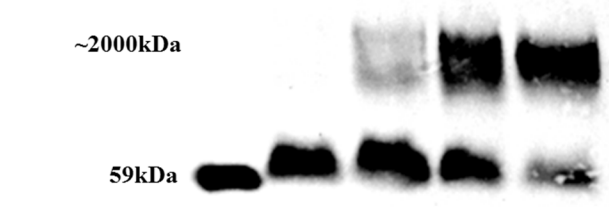

B

Lane	1	2	3	4	5
PFO(ng)	-	-	75	375	1500
PFO/C9T2(ng)	75	75	75	75	75
Membrane	-	+	+	+	+

Figure 4.

Ability of PFO/αT2 and PFO/C9T2 to form SDS-resistant oligomers on membranes. SDS-AGE analysis and western blotting with an anti His-tag antibody were used to examine SDS-resistant oligomer formation by PFO/αT2 and PFO/C9T2 on rabbit ghost membranes. (A) PFO/αT2 incubated in the absence or presence of ghost membranes and with or without PFO. Controls using up to 5 ug of PFO alone showed no signal (data not shown). (B) Same experiment performed with PFO/C9T2.

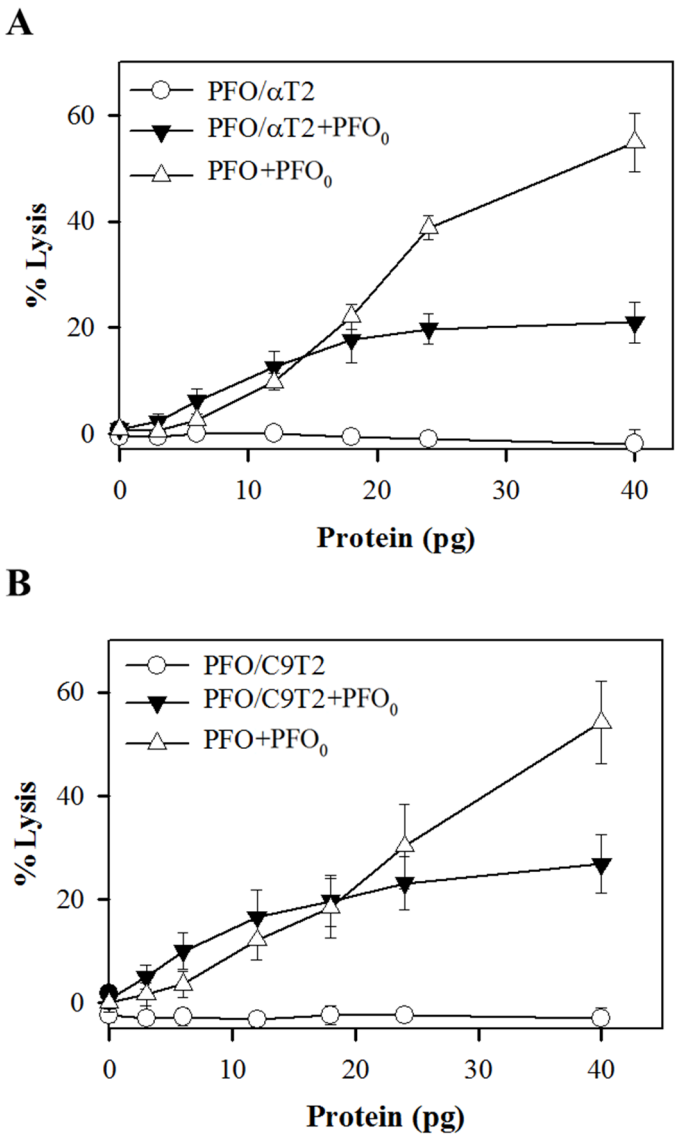

Figure 5.

Hemolytic activity of mixed complexes formed with PFO/αT2 or PFO/C9T2 and PFO. All assays except the chimeras alone, contained a fixed amount (3.6 pg) of PFO at a sublytic level that produced no detectable activity (PFO_0). Increasing amounts of PFO/αT2 or PFO/C9T2 were added at levels that also showed no activity alone. PFO was used as a control. (A) Results for PFO/αT2. (B) Results for PFO/C9T2.

Table 1

Hemolytic Activity of PFO Chimeras.

Chimera	Substitution in PFO[a]		Percent Activity (± 3%)
	TMH1	TMH2	
PFO			100
PFO/αT1	C8α (201–256)		0
PFO/αT2		C8α (329–385)	13
PFO/αT1, T2	C8α (201–256)	C8α (329–385)	*b*
PFO/C9T1	C9 (197–270)		*b*
PFO/C9T2		C9 (343–400)	11
PFO/C9T1, T2	C9 (197–270)	C9 (343–400)	*b*

[a] Substituted TMH1 and TMH2 segments of PFO correspond to residues 158–191 and 256–287, respectively.

[b] Could not be expressed in soluble form.